THE JOURNAL OF BIOLOGICAL CHEMISTRY VOL. 285, NO. 45, pp. 34875–34884, November 5, 2010

Integrin β_3 Phosphorylation Dictates Its Complex with the Shc Phosphotyrosine-binding (PTB) Domain*[S]

Received for publication, June 28, 2010, and in revised form, July 30, 2010 Published, JBC Papers in Press, August 25, 2010, DOI 10.1074/jbc.M110.159087

Lalit Deshmukh[‡], **Vitaliy Gorbatyuk**[§], **and Olga Vinogradova**[‡1]

From the [‡]*Department of Pharmaceutical Sciences, School of Pharmacy, and the* [§]*BioNMR Facility, Biotechnology-Bioservices Center, University of Connecticut, Storrs, Connecticut 06269-3092*

Adaptor protein Shc plays a key role in mitogen-activated protein kinase (MAPK) signaling pathway, which can be mediated through a number of different receptors including integrins. By specifically recognizing the tyrosine-phosphorylated integrin β_3, Shc has been shown to trigger integrin outside-in signaling, although the structural basis of this interaction remains nebulous. Here we present the detailed structural analysis of Shc phosphotyrosine-binding (PTB) domain in complex with the bi-phosphorylated $\beta_3$integrin cytoplasmic tail (CT). We show that this complex is primarily defined by the phosphorylation state of the integrin C-terminal Tyr^{759}, which fits neatly into the classical PTB pocket of Shc. In addition, we have identified a novel binding interface which concurrently accommodates phosphorylated Tyr^{747} of the highly conserved NP*X*Y motif of β_3. The structure represents the first snapshot of an integrin cytoplasmic tail bound to a target for mediating the outside-in signaling. Detailed comparison with the known Shc PTB structure bound to a target TrkA peptide revealed some significant differences, which shed new light upon the PTB domain specificity.

Integrins, a major class of non-covalent heterodimeric, glycoprotein cell surface receptors, are among the most studied and best characterized cell adhesion molecules. Integrins mediate a plethora of cell-cell, cell-extracellular matrix (ECM),[2] and cell-pathogen interactions and hence are responsible for controlling a wide array of biological processes including homeostasis, cell migration, differentiation, adhesion, immune response etc. The unique bidirectional flow of information through integrins involves inside-out signals, which allow them to interact with extracellular ligands (such as fibrinogen, von Willebrand factor, fibronectin) and ligand-dependent outside-in signals which adjust the cellular response to cell-cell adhesion (1). Although our understanding of the molecular details of inside-out integrin signaling (2, 3) has grown by leaps and bounds over the past decade, the early intracellular events following the integrin-mediated ECM engagement, outside-in signal transduction, still require further clarification. With respect to the outside-in signaling, the important unanswered questions center on selective recognition of proximal effectors by integrin cytoplasmic domains at different stages of cell spreading. Phosphorylation of the integrin tails is considered to be one of the spatiotemporal mechanisms for imparting such selectivity and, indeed, phosphorylation switches are thought to be a common principle of integrin regulation. Platelet integrin β_3 cytoplasmic tail (CT) is laden with various phosphorylation sites, including two tyrosines, one serine, and multiple threonines. However, only tyrosine phosphorylation is found to be specific for the outside-in signaling (4–8) and Shc (in particular its p52 isoform) was identified as a primary signaling partner for the tyrosine-phosphorylated β_3CT (8).

Adaptor protein Shc (Src homology 2 domain) plays a key role in mitogen-activated protein kinase (MAPK) signaling pathway (9) and can be recruited through many different types of receptors, including integrins, growth factor, antigen, cytokine, G-protein-coupled, and hormone receptors (10). In the context of the present study, it is important to mention that Shc has also been coupled to the integrin controlled cell cycle progression (11). One of the three isoforms, the p52 Shc contains three distinct domains: phosphotyrosine-binding (PTB) domain, a poorly characterized glycine/proline-rich region termed as collagen homology domain (CH1), and the SH2 domain. Previous studies have shown that two of these domains, PTB and SH2, could potentially interact with β_3CT containing phosphorylated tyrosines (12, 13). However, based on *in vitro* peptide affinity chromatography assays, Higashi *et al.* (14) proved that p52 Shc binds to the tyrosine-phosphorylated β_3 peptide through its PTB domain.

Overall, PTB domains comprise a large family of protein binding modules, which exhibit a conserved structural architecture similar to the pleckstrin homology (PH) domains (also termed as PH domain superfold) consisting of a core β-sandwich made of two anti-parallel β sheets flanked by a C-terminal helix. In terms of the PTB domain ligand specificity, although

* The work was supported in part by AHA grants (to O. V.).

The atomic coordinates and structure factors (code 2L1C) have been deposited in the Protein Data Bank, Research Collaboratory for Structural Bioinformatics, Rutgers University, New Brunswick, NJ (http://www.rcsb.org/).

Coordinates for Shc PTB-BPβ_3Peptide complex and the NMR data (NMR restraints, T_1, T_2, hetero-NOE values, and chemical shifts) were submitted to the Biological Magnetic Resonance Bank (BMRB entry: 17080).

[S] The on-line version of this article (available at http://www.jbc.org) contains supplemental Figs. S1–S4.

[1] To whom correspondence should be addressed: Dept. of Pharmaceutical Sciences, 69 North Eagleville Rd., Unit 3092, Storrs, CT 06269-3092. Tel.: 860-486-2972; Fax: 860-486-6857; E-mail: olga.vinogradova@uconn.edu.

[2] The abbreviations used are: ECM, extracellular matrix; PTB, phosphotyrosine-binding; CT, cytoplasmic tail; Shc, Src homology 2 domain; PH, pleckstrin homology; NMR, nuclear magnetic resonance; NOE, nuclear Overhauser effect; pY/Ptr, phosphorylated tyrosine; DSS, 4,4-dimethyl-4-silapentane-1-sulfonic acid; HSQC, heteronuclear single quantum correlation; mProxyl, 3-maleimido-PROXYL; PRE, paramagnetic relaxation enhancement; TCEP, tris(2-carboxyethyl)phosphine; TrkA, tyrosine kinase receptor; R.M.S.D., root mean square deviation; PDB, Protein Data Bank; BMRB, Biological Magnetic Resonance Bank.

phosphorylated tyrosine is required for high affinity binding in case of proteins such as Shc PTB, IRS-1/IRS-2/IRS-3, Dok1, and SNT/FRS2, the PTB domains of Dab1/Dab2, ARH, Fe65, ICAP1α, JIP-1/JIP-1b, Numb, Talin, and X11α exhibit similar or in some cases even higher affinity for non-phosphorylated peptides (15). For Shc PTB-integrin interaction, a bi-phosphorylated (pY^{747} and pY^{759}) peptide has been shown to have greater binding affinity than a mono-phosphorylated (pY^{759}) peptide (8). However, the exact structural basis underlying the second phosphotyrosine-binding site in a canonical PTB domain is not clearly understood.

Pathologically, Shc phosphorylation is linked to the stimulation of vascular endothelial growth factor (VEGF) production in tumors (16). Thus, deciphering the molecular details of this interaction may influence the development of new anti-cancer therapeutic strategies. Here we present the NMR-derived atomic view of how tyrosine phosphorylation affects β_3CT interaction with Shc PTB, and we show for the first time a high resolution three-dimensional structure of Shc PTB domain in complex with bi-phosphorylated integrin β_3CT peptide.

EXPERIMENTAL PROCEDURES

Expression and Purification—Cloning, expression, and purification of β_3CT have been described previously (2). Tyrosine phosphorylation was achieved *in vivo* by expressing β_3CT in TKB1 cell line from Stratagene. Details of this procedure and purification are described elsewhere.[3] The Shc PTB domain (residues 17–207, see Fig. 1*A*) containing pET15b vector, generously provided by Dr. Zhou, was expressed in Rosetta (DE3) cell line from Novagen to improve the expression levels. These cells express rare tRNAs facilitating the translation of genes that encode rare *Escherichia coli* codons. Purification of Shc PTB domain was performed according to the protocol from Qiagen under nondenaturing conditions followed by gel-filtration on HiLoad 16/60 Superdex 75 column in 50 mM Na_2HPO_4, 50 mM NaCl, 5 mM DTT buffer at pH 6.5. Short tyrosine(s)-phosphorylated peptides corresponding to mono- and bi-phosphorylated β_3CT, MPNβ_3, MPCβ_3, and BPβ_3 Peptide (Fig. 1*B*), were chemically synthesized (Genemed Synthesis, Inc.; NEO-peptides, Inc.).

NMR Sample Preparation—The heteronuclear NMR experiments were performed on uniformly ^{15}N and/or ^{13}C labeled, ~0.5 mM Shc PTB samples (unless mentioned otherwise), with or without the ligands/peptides on Varian Inova 600 MHz equipped with inverse-triple resonance cold probe at 35 °C. The samples were prepared in pH 6.5 (unless mentioned otherwise) buffer containing 50 mM Na_2HPO_4, 50 mM NaCl, 5 mM DTT, 7% D_2O, and 1 mM DSS acting as an internal standard. Chemical shift titration experiments between ^{15}N-labeled full-length β_3 CTs and non-labeled Shc PTB and ^{15}N-labeled Shc PTB and non-labeled full-length β_3 CTs were performed at pH 6.1 to avoid precipitation of β_3 CT.

NMR Spectroscopy—Chemical shifts assignments for the free form Shc PTB were obtained from BMRB Entry 5566 (17) and have been modified to match our construct and experimental conditions with the help of triple resonance NMR experiments,

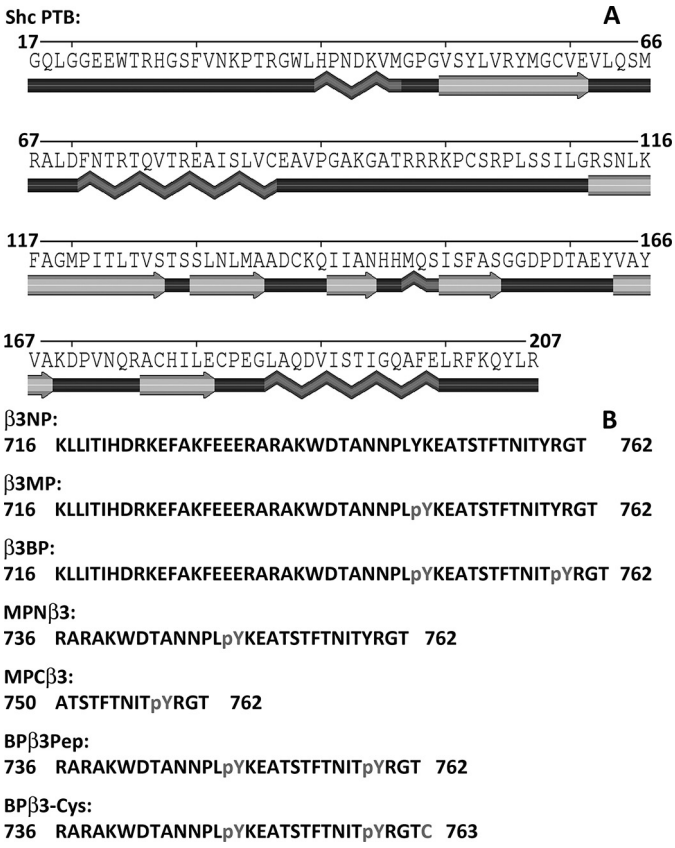

FIGURE 1. **The amino acid composition of Shc PTB (*A*) and integrin β_3 constructs (*B*) used for this study.** Polyview 2D (41) is used for generating two-dimensional secondary structural representations for Shc PTB. pY (shown in *gray*) represents phosphorylated tyrosine.

HNCACB and HNCO. For Shc PTB-BPβ_3Peptide complex (1:2 ratio), the backbone and side chain ^1H, ^{15}N, ^{13}C resonance assignments were made by using the standard triple resonance NMR experiments, namely HNCA, HNCACB, HNCO, HBHA-(CO)NH, and HNCACO. The intra-molecular NOE distance restraints were obtained from ^{13}C- and ^{15}N-edited three-dimensional NOESY-HSQC experiments and ^{13}C-edited aromatic three-dimensional NOESY-HSQC experiments (mixing time 150 ms). The inter-molecular NOE distance restraints between Shc PTB and BPβ_3Peptide were obtained from F1 ^{13}C,^{15}N-filtered, F2 ^{13}C-edited NOESY-HSQC spectrum (18, 19). Sequence-specific assignments of the non-phosphorylated and phosphorylated[3] integrin tails are described elsewhere (2) and have been modified to match changes in experimental conditions (pH, temperature and salt). The ^1H resonance assignments for BPβ_3Peptide in complex with Shc PTB were obtained from two-dimensional ^{13}C,^{15}N-filtered TOCSY and two-dimensional ^{13}C,^{15}N-filtered NOESY experiments (mixing time 65, 75 ms for TOCSY and 300, 400 ms in case of NOESY experiments). All the spectra were processed with NMRPipe (20) and/or Rnmrtk (21) and were analyzed by CCPN software suite (22). For the NMR dynamics study, ^1H-^{15}N NOE, ^{15}N T_1 and T_2 data were collected on Varian Inova 600 MHz spectrometer using the scheme adopted from L. Kay (23). ^{15}N T_1 values were measured from the spectra recorded with 16 different durations of the delay: $T = 0$, 10, 60, 150, 250, 370, 530, 760, 1150, 1350, 1550, 1750, 1950, 2150, 2500, and 3000 ms. ^{15}N T_2 values were

[3] O. Vinogradova, manuscript submitted.

determined from spectra recorded with 8 different durations of the delay: $T = 10$, 30, 50, 70, 90, 110, 130, and 150 ms. Steady-state heteronuclear ^{1}H-^{15}N NOE values were determined from spectra recorded with 5 s relaxation delay and the presence and absence of a proton presaturation period of 5 s. T_1, T_2, and NOE values were extracted by a curve-fitting subroutine included in the CCPN software suite (22). For curve fitting analysis, the spectra were processed with 10 Hz exponential broadening in direct dimension and zero-filled to 2048 × 1024 data points in *t*2 and *t*1, respectively.

Paramagnetic Labeling—To introduce a spin label, a new peptide, BPβ_3Cys, was chemically synthesized (NEO-peptides, Inc.) with an additional cysteine residue at the C terminus (Fig. 1*B*). A typical spin labeling reaction involved 50 mM Na_2HPO_4, 50 mM NaCl at pH 6.5, ~0.4 mM BPβ_3Cys, and ~5 mM cysteine-specific spin label, 3-maleimido-PROXYL (Sigma-Aldrich), hereafter referred to as mProxyl. The reaction was allowed to proceed for 1 h at room temperature. The unreacted mProxyl was then removed from mProxyl-BPβ_3Cys by using combination of gel-filtration chromatography on HiLoad 16/60 Superdex 75 column in 50 mM Na_2HPO_4, 50 mM NaCl at pH 6.5 and reverse phase HPLC on PROTO C4 column (The Nest Group, Inc.). ^{15}N HSQC spectrum was collected on sample containing 0.18 mM spin-labeled peptide (mProxyl-BPβ_3Cys) mixed with 0.1 mM ^{15}N Shc PTB in 50 mM Na_2HPO_4, 50 mM NaCl, 1 mM TCEP, 7% D_2O, 1 mM DSS buffer at pH 6.5 and 35 °C. An additional ^{15}N HSQC spectrum on the ^{15}N-labeled Shc PTB: BPβ_3Cys (same concentration and in same buffer as the paramagnetic sample) was collected for comparison. The ^{1}H,^{15}N resonance assignments of Shc PTB were modified to match these experimental conditions. For calculating the intensity ratios, again the spectra were processed with 10 Hz exponential broadening in direct dimension and zero-filled to 2048 × 1024 data points in *t*2 and *t*1, respectively.

Structure Calculation—The backbone, ϕ and ψ, dihedral angle restraints were obtained by using Talos+ (24). Initial structure calculations were performed by using CYANA 2.1 (25). Hydrogen bond restraints were introduced during the final stages of calculations based on secondary structure elements identified from previous rounds of structure calculations. Eighty lowest energy structures from CYANA were then subjected to molecular dynamics simulations in explicit water (26) using CNS (27). Table 1 lists detailed structural statistics of the final 15 lowest energy conformers after the water refinement. None of the structures have NOE and dihedral angle violations more than 0.5 Å and 5°, respectively. The Protein Structure Software suite (PSVS; courtesy of CABM Structural Bioinformatics Laboratory, Rutgers, State University of New Jersey) was used for structure quality assessment and validation.

RESULTS

β_3CT Interaction with Shc PTB Domain Strongly Depends on the Phosphorylation State of Its Tyrosines—Previous biochemical studies have indicated that p52 isoform of Shc co-immunoprecipitates with tyrosine-phosphorylated $\alpha_{IIb}\beta_3$ from the aggregated platelets and that Shc itself gets tyrosine phosphorylated during platelet aggregation (6). This p52 isoform of Shc binds to the tyrosine-phosphorylated β_3 peptide through its PTB domain (14) and phosphorylation of Tyr^{759} of β_3CT is essential to meditate this interaction as only the peptides containing pY^{759} have shown affinity toward GST-fused Shc (8). To further confirm and structurally characterize these findings, we have employed Nuclear Magnetic Resonance spectroscopy (NMR). To pinpoint the residues/regions involved in the Shc PTB-β_3CT interaction, we began with the chemical shift mapping experiments. Non-labeled Shc PTB domain was mixed with ^{15}N-labeled non-phosphorylated β_3CT (hereafter referred to as β_3NP), Tyr^{747} mono-phosphorylated β_3CT (hereafter referred to as β_3MP) and ^{747}Y-^{759}Y bi-phosphorylated β_3CT (hereafter referred to as β_3BP) at the ratio 2:1 and the associated chemical shifts perturbations were monitored (expanded regions of superimposed HSQC spectra are shown in Fig. 2: (*A*) β_3NP; (*B*) β_3MP, and (*C*) β_3BP). As expected, Shc PTB addition had no effect on HSQC spectrum of β_3NP. In contrast, both β_3MP and β_3BP HSQC spectra show significant differential line-broadening and several peaks disappearance along with some small shifts in resonance frequencies upon addition of Shc PTB (with an exception of the very last C-terminal residue Thr^{762} of β_3BP, which demonstrates substantial chemical shift, Fig. 2*C*). This phenomenon is probably due to the intermediate exchange between free and bound states of β_3MP and β_3BP (28) combined with relatively large molecular weight of the complex (about 33 kDa complex *versus* 8 kDa for β_3CT alone). The ratio of the peak intensities along with chemical shifts perturbations for β_3MP and β_3BP residues plotted as a function of residue numbers is shown in Fig. 2, *D* and *E*, respectively. Combination of the differential line broadenings and chemical shift perturbations suggests the regions involved in interaction between phosphorylated β_3CT and Shc PTB, namely (i) residues from Asp^{740} to Ala^{750}, surrounding $^{744}NPLpY^{747}$ motif, in case of β_3MP, and (ii) almost the entire C terminus, extending from Asp^{740} to Gly^{762} and encompassing both $^{744}NPLpY^{747}$ and $^{756}NITpY^{759}$ motifs plus the region connecting them in case of β_3BP. Because the affected region for β_3BP upon Shc PTB addition is much broader than the one for β_3MP, it can be argued that the binding site around $^{744}NPLpY^{747}$ motif is a complimentary one and serves to stabilize β_3CT orientation within the complex which has been defined by the primary binding site around $^{756}NITpY^{759}$ motif.

To confirm the hypothesis that $^{756}NITpY^{759}$ motif occupies the canonical PTB site and to map the residues involved from Shc PTB side, we performed similar chemical shift mapping experiments. Non-labeled β_3NP, β_3MP, β_3BP solutions were mixed with ^{15}N-labeled Shc PTB at the ratio 2:1. The superimposition of expanded regions of HSQC spectra for ^{15}N-labeled Shc PTB mixed with β_3 NP, MP, BP is depicted in Fig. 3*A* (Shc PTB alone is shown in *black*; with β_3NP, in *blue*; β_3MP, in *red*; and β_3BP, in *lime*; the superimposition of entire spectra is presented in supplemental Fig. S1*A*). As predicted, there were no changes in the ^{15}N-labeled Shc PTB HSQC spectrum upon addition of the full-length non-labeled β_3NP. Addition of β_3MP to ^{15}N-labeled Shc PTB leads to several small shifts in resonance frequencies as well as appearance of few additional (doublet) weak peaks probably representing a small population of protein in bound conformation. In contrast, there are signifi-

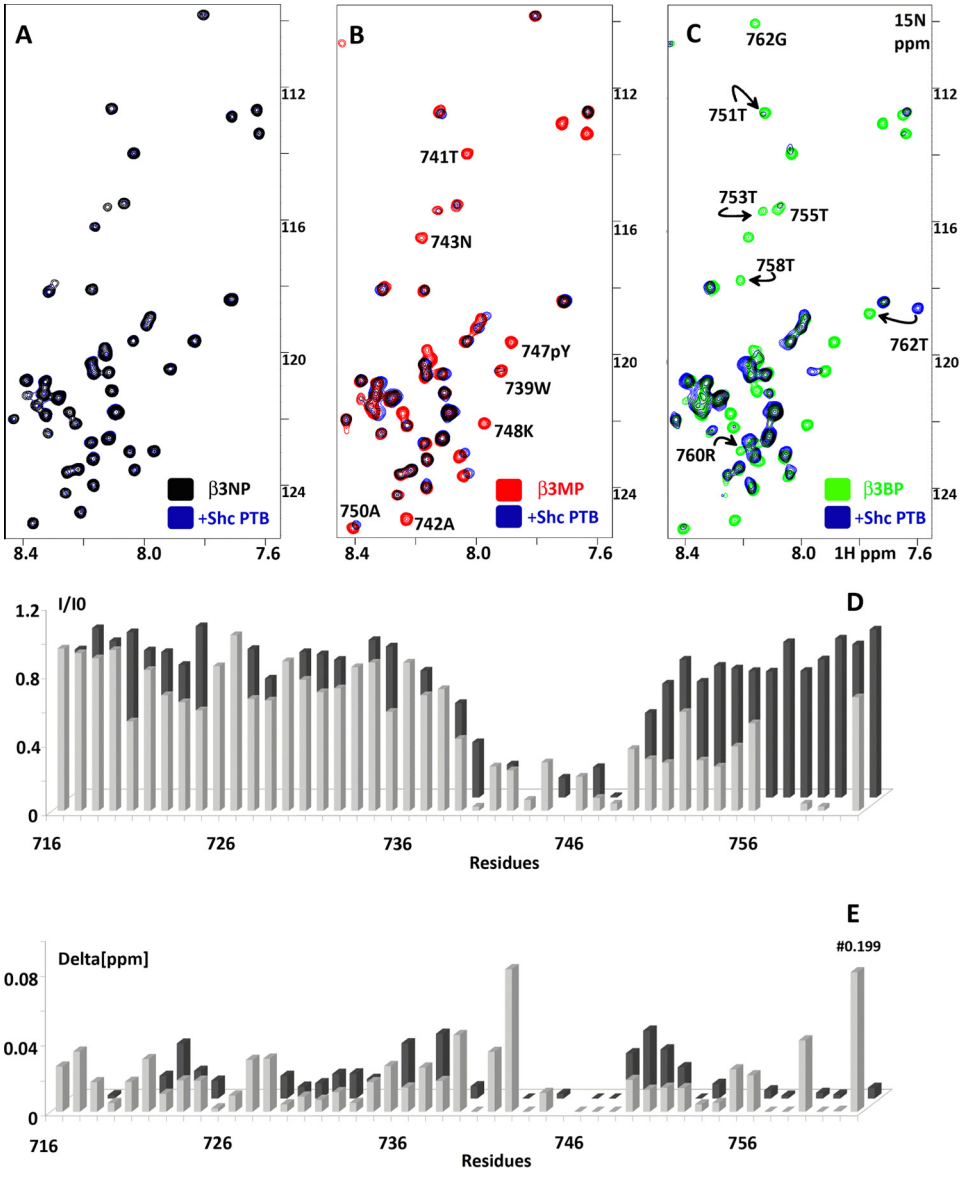

FIGURE 2. **Summary of ^{15}N-labeled β_3NP, MP, BP, and non-labeled Shc PTB interactions.** The superimposition of ^{15}N-^{1}H HSQC spectra of ^{15}N-labeled (*A*) β_3NP (*black*) in the presence of Shc PTB (*blue*); (*B*) β_3MP (*red*) in the presence of Shc PTB (*blue*); (*C*) β_3BP (*lime*) in presence of Shc PTB (*blue*); important residues are labeled and marked with *arrows*; (*D*) normalized intensity ratios (I/I_0) of the ^{15}N-labeled β_3MP, β_3BP with and without non-labeled Shc PTB plotted as a function of residue number; (*E*) chemical shift changes of ^{15}N-labeled β_3MP, β_3BP due to the addition of non-labeled Shc PTB. The column height for residue Thr^{762} in case of ^{15}N-labeled β_3BP+ non-labeled Shc PTB (Delta [ppm] of 0.199 ppm) has been truncated for the sake of clarity. Bars are colored as follows: β_3MP (*dark gray*) and β_3BP (*light gray*). Delta [ppm] refers to the combined HN and N chemical shift changes, according to the equation: $\Delta\delta(HN,N) = ((\Delta\delta HN^2 + 0.2(\Delta\delta N)^2)^{1/2}$, where $\Delta\delta = \delta_{bound} - \delta_{free}$. All the experiments were performed at 35 °C and at pH 6.1, in the buffer containing 50 mM Na_2HPO_4, 50 mM NaCl, 5 mM DTT, 7%D_2O, and 1 mM DSS.

cant changes in HSQC spectrum of Shc PTB upon addition of β_3BP indicating substantial conformational rearrangement of Shc PTB, a hallmark of Shc PTB domain (17). However, low mutual solubility of Shc PTB and full-length β_3CT constructs prevented us from conducting a full scale, thorough NMR structural investigation of Shc PTB-β_3BP interaction.

To circumvent the solubility issue and to understand this interaction in atomic details, we have synthesized three phosphorylated tyrosines containing peptides representing different regions of the full-length β_3CT, which are involved in interaction with Shc PTB (Fig. 1*B*). Similar chemical shift mapping experiments were performed on ^{15}N-labeled Shc PTB mixed with non-labeled N-terminal mono-phosphorylated peptide, MPNβ_3, C-terminal mono-phosphorylated peptide, MPCβ_3, and C-terminal bi-phosphorylated peptide, BPβ_3Peptide. Chemical shifts perturbations were monitored and are depicted in Fig. 3*B* (superimposition of the full spectra is presented in supplemental Fig. S1*B*). The outcome appeared to be very similar to the full-length β_3CT titrations. (The complete chemical shift perturbations, *i.e.* ^{15}N-labeled Shc PTB + non-labeled MPNβ_3, MPCβ_3, BPβ_3Peptide, are presented in supplemental Fig. S1*C*). Addition of MPNβ_3, containing pY^{747}, leads to small shifts in Shc amide resonance frequencies together with an appearance of several weak doublet peaks. Based upon this observation, we can suggest that in the absence of pY^{759}, pY^{747} may occupy the orthodox PTB site. However, its higher dissociation rate may prevent the stabilization of the structural rearrangement in Shc PTB. In contrast, addition of MPCβ_3, containing pY^{759}, as well as addition of BPβ_3Peptide, containing both pY^{759} and pY^{747}, to Shc PTB results in significant perturbations in Shc PTB HSQC spectrum. Overall, these perturbations resemble very closely to the ones found in Shc PTB-TrkA complex (17) representing a very well established conformational rearrangement of Shc PTB upon ligand binding. Surprisingly and on a more important note, these titration experiments indicated that although MPCβ_3 alone is sufficient to induce the classical conformational change in Shc PTB, similar or even the greater conformational rearrangement is achieved via addition of BPβ_3Peptide. Fig. 3*C* depicts these crucial differences in chemical shifts perturbations between MPCβ_3 *versus* BPβ_3Peptide plotted as a function of Shc PTB residue number, which provides us with the essential information about the possible binding site for the ^{744}NPLpY^{747} motif. Explicitly, three Shc PTB regions are particularly different: (*a*) residues ^{78}T–E^{80} of the helix α2, (*b*) residues Arg^{104} and Leu^{106} of the long loop connecting helix α2 and strand β2 and (*c*) residues ^{159}D–V^{164} of the loop connecting strand β5-β6. Mapping these regions on the available Shc PTB structure (PDB ID: 1SHC) (12) suggests

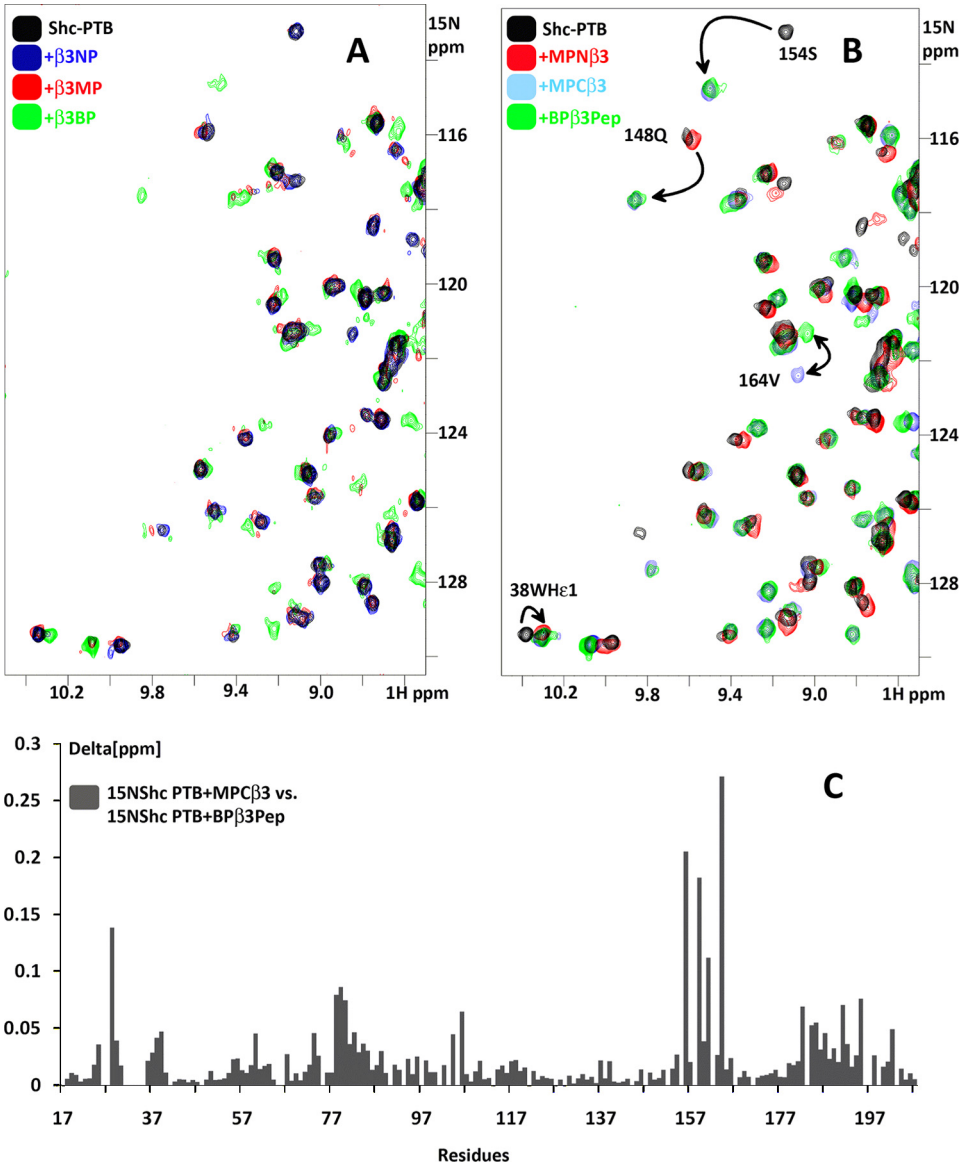

FIGURE 3. **Summary of ^{15}N-labeled Shc PTB and non-labeled β_3CT interactions.** *A*, superimposition of ^{15}N-^{1}H HSQC spectra of ^{15}N-labeled Shc PTB (*black*) in presence of non-labeled β_3NP (*blue*); β_3MP (*red*); β_3BP (*green*); pH 6.1; (*B*) superimposition of HSQC spectra of ^{15}N-labeled Shc-PTB (*black*) in presence of non-labeled MPNβ_3 (*red*); MPCβ_3 (*light blue*) and BPβ_3Peptide (*lime*); pH 6.5; Some of the important residues undergoing conformational change are labeled and marked with *arrows*; (*C*) chemical shift differences between ^{15}N-labeled Shc-PTB + MPCβ_3 *versus* ^{15}N-labeled Shc-PTB +BPβ_3Peptide. Delta [ppm] refers to the combined HN and N chemical shift changes, according to the equation: $\Delta\delta(HN,N) = ((\Delta\delta HN^2 + 0.2(\Delta\delta N)^2)^{1/2}$, where $\Delta\delta = \delta_{bound} - \delta_{free}$. All the experiments were performed at 35 °C, in the buffer containing 50 mM Na_2HPO4, 50 mM NaCl, 5 mM DTT, 7% D_2O, and 1 mM DSS.

that accommodation of ^{744}NPLpY^{747} motif requires some movement of the helix α2 and the flexible loop connecting α2 to β3 strand.

To conclude, our titrations results are in good correlation with Cowan *et al.* (8) demonstrating that the phosphorylation of Tyr^{759} β_3CT is essential to meditate direct integrin interaction with Shc PTB except that the NMR methods have allowed us to observe a weak interaction between Shc PTB and β_3 peptides containing only pY^{747}, which the biochemical assays could not detect.

Structural and Dynamic Characterization of the Complex—Based upon our titration experiments, we could predict the possible mode of interaction of Shc PTB with BPβ_3Peptide (27 residues, Fig. 1*B*): positively charged side-chain of Arg^{104} forming a salt-bridge with negatively charged phosphate group of pY^{747} whereas pY^{759} occupying the canonical PTB site. To fully characterize this interaction at atomic level, we have determined the three-dimensional solution structure of Shc PTB-BPβ_3Peptide complex using modern triple resonance NMR methods (described in details under "Experimental Procedures"). Inter-molecular NOEs were paramount in defining the orientation of BPβ_3Peptide within the complex, which was later independently confirmed by paramagnetic relaxation enhancement (PRE) experiments (see below). Table 1 summarizes the structural statistics for the final 15 water refined structures with lowest energies and Fig. 4, *A* and *B* depict the backbone superimposition and ribbon representation of these structures respectively (the secondary structural features are presented in supplemental Fig. S2).

As seen in case of Shc PTB-TrkA complex, the N-terminal region of Shc PTB (residues 17–35) are dynamically unstructured (12), whereas the core-structured region of Shc PTB, encompassing residues 38–201, adopts a well known PH domain superfold in complex with BPβ_3Peptide: a seven-stranded β-sandwich composed of two anti-parallel β-sheets capped by a C-terminal α-helix (α3). Moreover, it contains two additional α-helices, N-terminal α1 and α2 connected to strands β1 and β2 respectively. Examination of this complex reveals the details of the binding sites for both pYs (Fig. 4*C*). As expected, residues ^{754}FTNITpY^{759} (representing the classical consensus φxNPxpY Shc PTB recognition motif with an exception of an isoleucine replacing proline residue) sits in the canonical PTB grove, an elongated cleft located between helix α3 and stand β5, with negatively charged phosphate group forming salt-bridges with positively charged side chains/amides of the Arg^{67}, Arg^{175}, Lys^{169}, and Gln^{148}. The residues ^{752}STF^{754} of BPβ_3Peptide adopt an anti-parallel β-strand conformation aligned to β5 strand of Shc PTB with hydrophobic amino acid, Phe^{754}, maintaining the majority of inter-subunit contacts. In fact, we can suggest that this large hydrophobic residue, Phe^{754}, is crucial for directing C-terminal pY^{759} into the canonical PTB pocket: compared with Ala^{742}, the

TABLE 1
Structural statistics of Shc PTB-β_3 integrin complex

Distance restraints		
All	:	4196
Short range (i-j < = 1)	:	1793
Medium-range (1 < i-j < 5)	:	699
Long-range (i-j > = 5)	:	1704
Intra-β_3	:	324[a]
Shc PTB-β_3	:	241[b]
Dihedral angle restraints		
Phi (ϕ)	:	218[c]
Psi (ψ)	:	218[c]
Hydrogen bond restraints[d]		
Total	:	166
Intra-Shc PTB	:	152
Intra-β_3	:	1
Shc PTB-β_3	:	13
Average CYANA target function value	:	7.59
Violations		
NOE	:	0.0253 ± 0.0012
cdih	:	0.4003 ± 0.0549
RMSD (Å)[e]	:	
Average backbone RMSD to mean	:	0.5
Average heavy atom RMSD to mean	:	1.0
Van der Waals energy (kcal mol^{-1})[f]	:	−1930.90 ± 66.72
Deviation from idealized geometry		
Bonds (Å)	:	0.0045 ± 0.00011
Angles (°)	:	0.5881 ± 0.0159
Impropers (°)	:	1.5694 ± 0.0709
Ramchandran statistics (%)[g]		
Residues in most favored regions	:	72.9
Residues in additional allowed regions	:	25.0
Residues in generously allowed regions	:	2.1
Residues in disallowed regions	:	0

[a] Based upon two-dimensional ^{13}C,^{15}N-filtered NOESY.
[b] Based upon F1 ^{13}C, ^{15}N-filtered, F2 ^{13}C-edited NOESY-HSQC, and ^{15}N-edited NOESY and ^{13}C-edited NOESY.
[c] Generated from Talos+ (24).
[d] Hydrogen bonds were introduced in the last stage of structure calculations.
[e] Residues 36–202 (Shc PTB), 740–760(BPβ_3Peptide) calculated using PSVS.
[f] After refinement in explicit water by using CNS (27).
[g] All residues.

pY-5 residue in case of ^{744}NPLpY^{747} motif, it has the ability to accommodate more essential core hydrophobic contacts. Residues ^{756}NITpY^{759} form a type-I β turn, which is further stabilized by N^{756}–F^{198} contacts.

The binding site for the second pY^{747} is located in the grove formed between helix α2 and long flexible loop connecting the strand β2 and helix α2. Similar to the ^{756}NITpY^{759} motif, ^{744}NPLpY^{747} motif forms a type-I β turn which fits nicely into the pocket formed by residues ^{100}KPCSRPLS^{107}. Although ^{97}R-R^{99} containing region is highly flexible (see the relaxation data below), the prolines in ^{100}KPCSRPLS^{107} motif give rigidity to this phosphotyrosine-binding grove where the pY^{747} interacts with the positively charged side chain of Arg^{104}. This interaction is further stabilized by contacts between ^{107}S-A^{742} and ^{107}S-T^{741} (see supplemental Fig. S3 for representative intermolecular NOEs) and salt bridges between side chain of Gln^{76} and Ala^{742}. The region connecting these two phosphotyrosine motifs, ^{749}E-T^{753} is stretched across one face of Shc PTB β-sandwich (β5, β6, α2) defined by the intermolecular NOEs between A^{750}-R^{79} and E^{749}-T^{75}. The N-terminal residues ^{736}RAKW^{739} of BPβ_3Peptide are dynamically unstructured and are not well defined. This ensemble, the NMR data and chemical shifts table have been deposited to Protein Data Bank (PDB) and Biological Magnetic Resonance Bank (BMRB) with the access codes 2L1C and 17080, respectively.

The BPβ_3Peptide orientation was further confirmed and validated by introduction of the cysteine specific paramagnetic spin label, mProxyl, attached to the C terminus of modified peptide, BPβ_3Cys, through the formation of thioether bond and measuring the distance-dependent reduction in peaks intensities in ^{15}N-labeled Shc PTB HSQC spectrum (29). These PRE studies independently confirmed the orientation of the phosphorylated integrin tail. Briefly, paramagnetic spin label facilitates nuclear relaxation in a distance-dependent manner ($1/r^6$), causing significant line-broadening for nuclei in proximity (<15–20 Å) to the free radical. Analysis of the reduction in NMR peaks intensities allows mapping the direct location of the spin label with respect to the protein binding surface (30). This pattern of reductions in peaks intensities of Shc PTB HSQC spectra upon addition of mProxyl-BPβ_3Cys is depicted in Fig. 5*D* and the intensities ratios are mapped on the surface of the complex in Fig. 4*D*. The affected residues are shown in color gradient from *orange* to *yellow* (most affected: *orange*, least affected: *yellow*), and residues for which we have no data are shown in *gray*. The expanded region of superimposed HSQC spectra is shown in supplemental Fig. S4. It should be noted that the chemical shift perturbations in Shc PTB resonances are very similar/almost identical upon addition of BPβ_3Peptide or modified BPβ_3Cys at 1:2 ratio indicating that the inclusion of an additional cysteine residue at the C terminus did not alter the bound conformation and/or the affinity of binding. The specific pattern of the altered cross-peak intensities, including the significant reduction in peak intensities (I_{para}/I_{dia} <0.3) of the ^{146}H-I^{150}, ^{168}A-V^{172}, ^{201}R-R^{207} regions indicates that the C-terminal mProxyl tag is, indeed, positioned near the canonical binding site. This confirms the occupancy of the binding pocket by pY^{759} and eliminates any possibility for the distant pY^{747} to be found at the same place.

Further, to better understand the backbone conformational flexibility of Shc PTB in complex with β_3 integrin, we have measured the relaxation parameters T_1, T_2, and heteronuclear ^{1}H-^{15}N NOEs (Fig. 5, *A*–*C*). The average value of T_1 is about 710 ms; the average value of T_2 is about 50 ms; and the average NOE value is about 0.66. For most of the residues, T_1 and T_2 values do not deviate significantly beyond the experimental error from the average numbers. However, several regions, including dynamically unstructured N-(residues 17–38) and C-(residues 202–207) termini plus a stretch of residues (91–100) within loop connecting helix α2 with strand β2 (89–111), demonstrate fast internal motion with increased T_2 and reduced NOE values. The flexible nature of this loop with the most profound motion associated with the residues Arg^{97} and Arg^{99} allows crucial structural changes to ensure the formation of the second phosphotyrosine-binding pocket. The motion of ^{100}KPCSRPLS^{107} region within this loop is restricted because of the interaction with β_3 ^{744}NPLpY^{747} motif.

DISCUSSION

The short cytoplasmic tails of integrins (see Fig. 6*E*), devoid of any intrinsic enzymatic activity and unable to connect directly to cytoskeleton, can interact with variety of adapter proteins via surprisingly few specific, highly conserved motifs. These include membrane-proximal region, HDRk/rE and/or

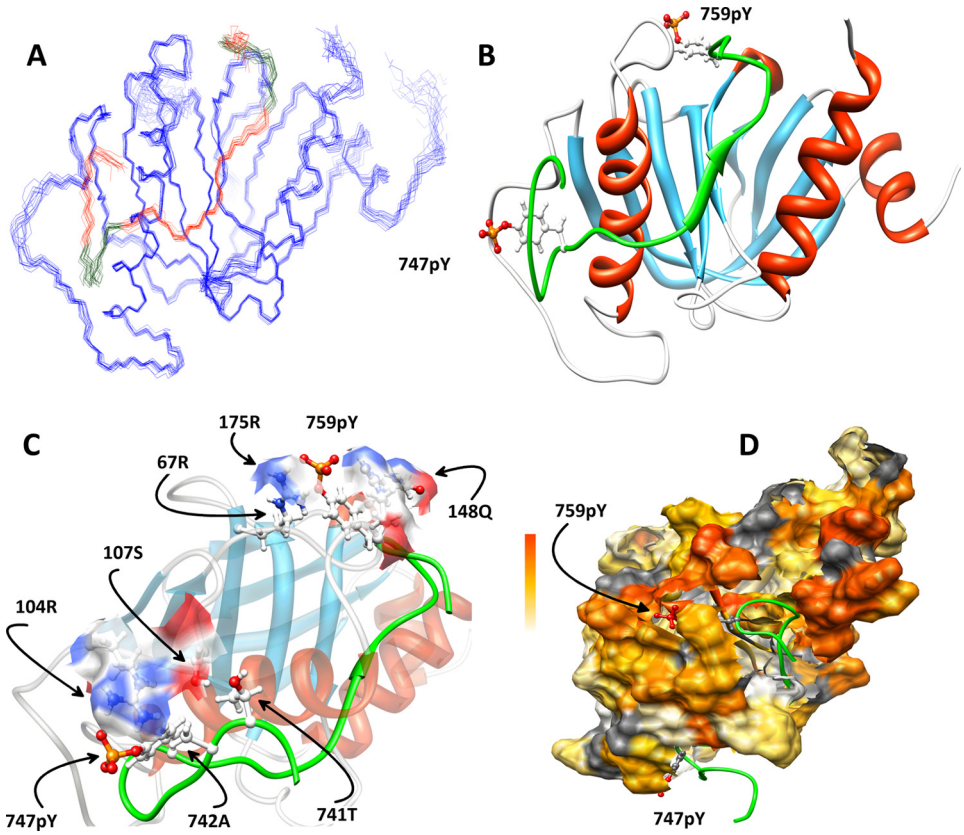

FIGURE 4. **Structure of Shc PTB-BPβ_3Peptide complex.** Molecular graphics images were produced using the UCSF Chimera package (42). Disordered regions (Shc PTB: 17–34, 203–207 and BPβ_3Peptide 736–739) are excluded for the sake of clarity. *A*, backbone superimposition of 15 lowest energy structures, the Shc PTB backbone is shown in blue and BPβ_3Peptide is shown in *red*. ^{744}NPLpY^{747} and ^{756}NITpY^{759} motifs are colored in *dark green*; *B*, ribbon diagram of conformer closest to the mean with the same view. BPβ_3Peptide is colored in lime, phosphorylated tyrosine residues (pY^{747}, pY^{759}) are shown with *ball* and *stick representation*; (*C*) binding interface between Shc PTB and BPβ_3Peptide. Important residues involved in the interaction are shown with *ball and stick representation* and in case of Shc PTB with an additional semi-transparent surface representation and are marked with *arrows*. Shc PTB is shown with *transparent ribbons*. The atoms and the surfaces are colored according to the electrostatic charges, *red*: negative, *blue*: positive, *white*: neutral; (*D*) surface representation of Shc PTB in complex with BPβ_3Peptide (depicted in *green ribbon*, phosphorylated tyrosine residues (pY^{747}, pY^{759}) are shown with *ball and stick representation*). The intensity ratios from the PRE experiment are mapped onto the surface of Shc PTB. *Orange* to *yellow* color gradient is used to map the intensities (*orange*: ~0, *yellow*: ~1). Residues with missing information and prolines are marked in *gray*.

one of the two N*XXY* motif containing regions recently reviewed in details (31). Overall, these interactions are tightly controlled with phosphorylation as one of the possible regulatory mechanisms. The phosphorylation state of the tyrosine residues within N*XXY* motifs of β_3CT can differentially regulate β_3 interactions with PTB domain-containing proteins. Talin, for example, serves as a major activator for non-phosphorylated β_3 (2, 32, 33), while Dok1 binds to pY^{747}-β_3 with higher affinity and, thus, replaces talin favoring the latent state of the receptor (34). Furthermore, Cowan *et al.* (8) have demonstrated that phosphorylation of the Tyr^{759} is essential for the direct Shc binding, which mediates outside-in signaling events (35). Until now, however, the detailed structural basis of this interaction has remained elusive. The present study exposes the exact molecular mechanism underlying the Shc PTB-β_3CT complex formation and takes our understanding of the nature of this interaction to a new level.

The NMR data presented unambiguously proves that both phosphorylated tyrosine residues are involved in interaction with Shc PTB domain, although the vital role is performed by pY^{759}. As depicted in Fig. 4, the BPβ_3Peptide wraps itself around Shc PTB with the major focal points presented by electrostatic interactions between negatively charged phosphate groups of pY^{759}/pY^{747} and positively charged side chains of Shc PTB (residues Arg^{67}, Arg^{175}, Lys^{169}, Gln^{148} in case of pY^{759} and Arg^{104} in case of pY^{747}). As predicted, ^{756}NITpY^{759} motif occupies the canonical PTB pocket with residues ^{752}STF^{754} forming an anti-parallel β strand against the β5 strand (^{150}ISFA^{153}) of Shc PTB. This complex also illuminates an additional novel binding site for pY^{747} with the characteristic, perpetual type-I β turn of ^{744}NPLpY^{747} motif fitting nicely into the grove formed between helix α2 and long flexible loop connecting the strand β2 and the helix α2.

A direct comparison between Shc PTB-BPβ_3Peptide complex and Shc PTB-TrkA complex (pdb id: 1SHC), depicted on Fig. 6*A*, reveals major similarities with some crucial differences depicted in Fig. 6*A*. Overall, the Cα atoms of the structured regions (residues 41–198) superimpose to the mean structure reasonably well with an R.M.S.D. of 2.26 Å ± 0.98Å. As presented in Fig. 6*B*, R.M.S.D. graph most of the β strands superimpose very well with an R.M.S.D. below 1 Å. The pY^{759} of β_3, occupying a canonical PTB site, overlaps neatly with pY^{490} of TrkA with small shifts in placement accompanied by corresponding movement of the loops connecting strands β4/β5 and β5/β6 (Fig. 6*C*). However, the regions involved in the formation of the second, pY^{747}, binding site show remarkable differences. The position of the loop connecting the helix α2 with the strand β2 is significantly different, reflecting the biggest fluctuation in the graph with maximum R.M.S.D. over 6 Å. Based upon our titration data and the previous biochemical assays (8), this novel phosphotyrosine-binding groove formed between the long loop and helix α2, is responsible for defining the precise arrangement of this large 27 residues bi-phosphorylated integrin constituent on Shc PTB surface, thereby increasing the binding affinity as compared with the small 11 residues, mono-phosphorylated (pY^{759}) MPCβ_3. So far the exact structural role of this unusually long loop (~24 residues), exclusively found in Shc PTB domain, has not been established except for residue Arg^{112}, situated at the beginning of β2 strand, which has been implicated in phospholipid interaction along with residues Lys^{116} and Lys^{139} (36). As per our knowledge, this is the first time when residues ^{100}KPCSRPLS^{107}

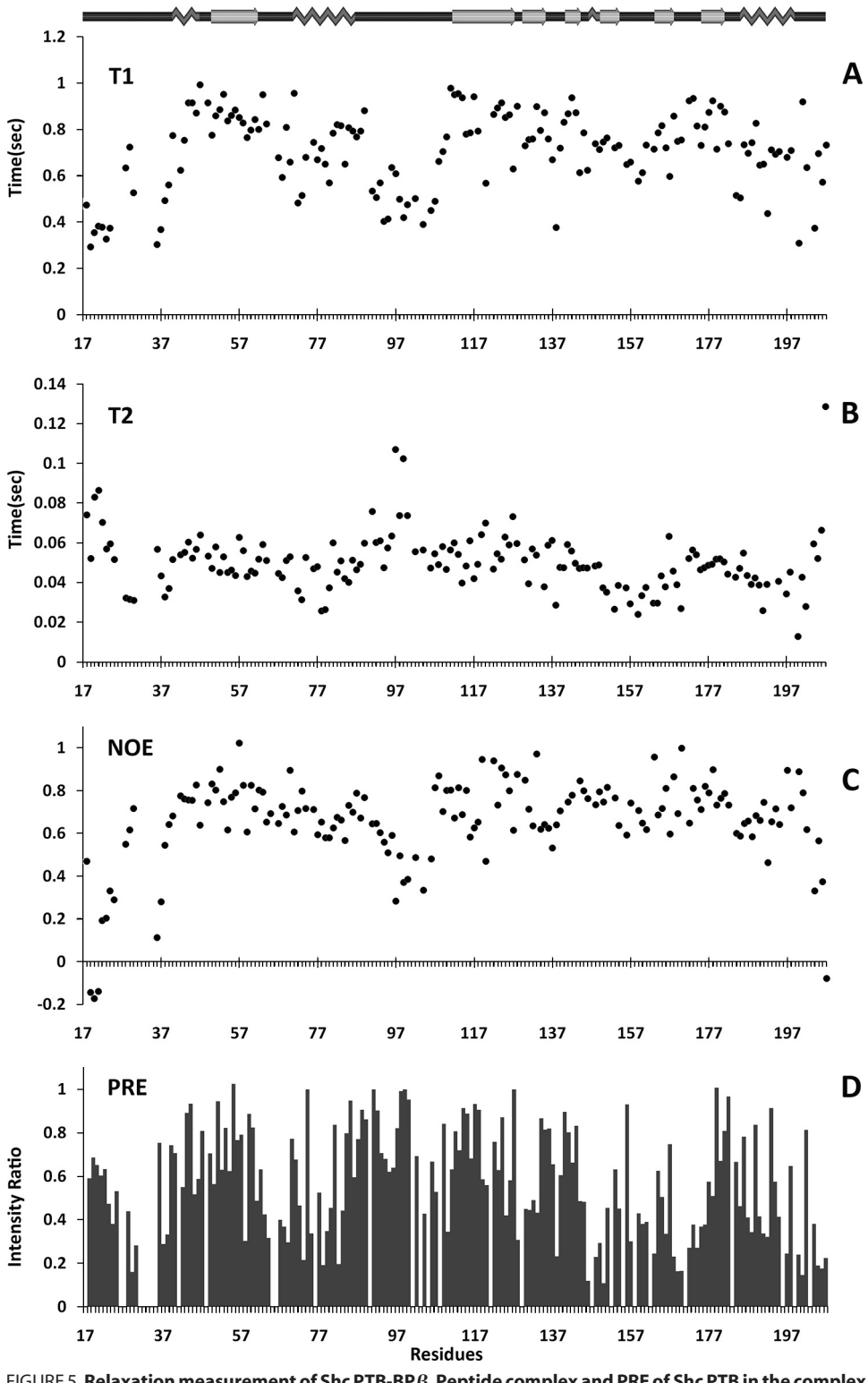

FIGURE 5. **Relaxation measurement of Shc PTB-BPβ_3Peptide complex and PRE of Shc PTB in the complex with mProxyl-BPβ_3Cys.** Secondary structural elements are represented above the T_1 plot. T_1 (*A*), T_2 (*B*), ^{15}N–^1H NOE (*C*) values of the backbone amide resonances of Shc PTB plotted against the residue numbers. *D*, normalized experimental intensity ratios ($Q = I_{para}/I_{dia}$) for Shc PTB backbone amide protons in the complex with paramagnetically (I_{para}) and diamagnetically (I_{dia}) labeled BPβ_3Cys plotted against residue numbers. An intensity ratio of one indicates no effect of the spin label on an amide proton. All the relaxation measurements were performed at 35 °C, pH 6.5 in the buffer containing 50 mM Na_2HPO_4, 50 mM NaCl, 5 mM DTT, 7% D_2O, and 1 mM DSS whereas PRE experiments were performed in the buffer containing 50 mM Na_2HPO_4, 50 mM NaCl, 1 mM TCEP, 7% D_2O, and 1 mM DSS.

of this elongated loop, commonly referred as Shc loop (37), are shown to be involved in direct interaction with a phosphorylated tyrosine residue. The actual biological significance of the proximity of these two binding sites, the phospholipid and the, pY^{747}, phosphotyrosine-binding site, is yet to be understood. However, this comparison between Shc PTB-TrkA and Shc PTB-BPβ_3Peptide, along with the NMR relaxation data, proves the flexible nature of Shc PTB loop(s) manifesting the versatility found in PTB fold.

To further analyze the capability of PTB domains to accommodate different fragments of integrin tails we compared the known structure of integrin β_3 (chimera, (34)) bound to talin (PDB ID: 1MK7) with Shc-β_3 complex. Talin PTB (also known as an F3 variant of the canonical PTB) domain differs significantly from Shc PTB, it is only about half in size (~100 residues long *versus* ~200) with missing analogs for helices α1 and α2 and the long Shc loop and with absolutely no sequence homology even within the canonical binding pocket. However, in terms of structural architecture, the core seven-stranded β-sandwich together with C-terminal α-helix of talin PTB-β_3 complex superimposes surprisingly well with Shc PTB-BPβ_3Peptide complex (see Fig. 6*D*), even though the residues defining the interaction from the β_3 side are completely different. In both cases, two different N*XXY* motifs of β_3 integrin form reverse turns which are further stabilized by contacts between N^{756}–F^{198} for Shc and N^{744}–T^{354}/I^{356} for talin. An aromatic residue Trp^{739} (at Y-8 position), as compared with the hydrophobic Ile^{485} of TrkA or Phe^{754} of β_3 integrin in the complex with Shc (both found in canonical pY-5 positions), defines the antiparallel orientation of the ligand β strand. Both these antiparallel β strands, formed by residues ^{752}STF^{754} in case of Shc and residues ^{739}WDTA^{742} in case of talin, superimpose surprisingly well. However, the non-phosphorylated

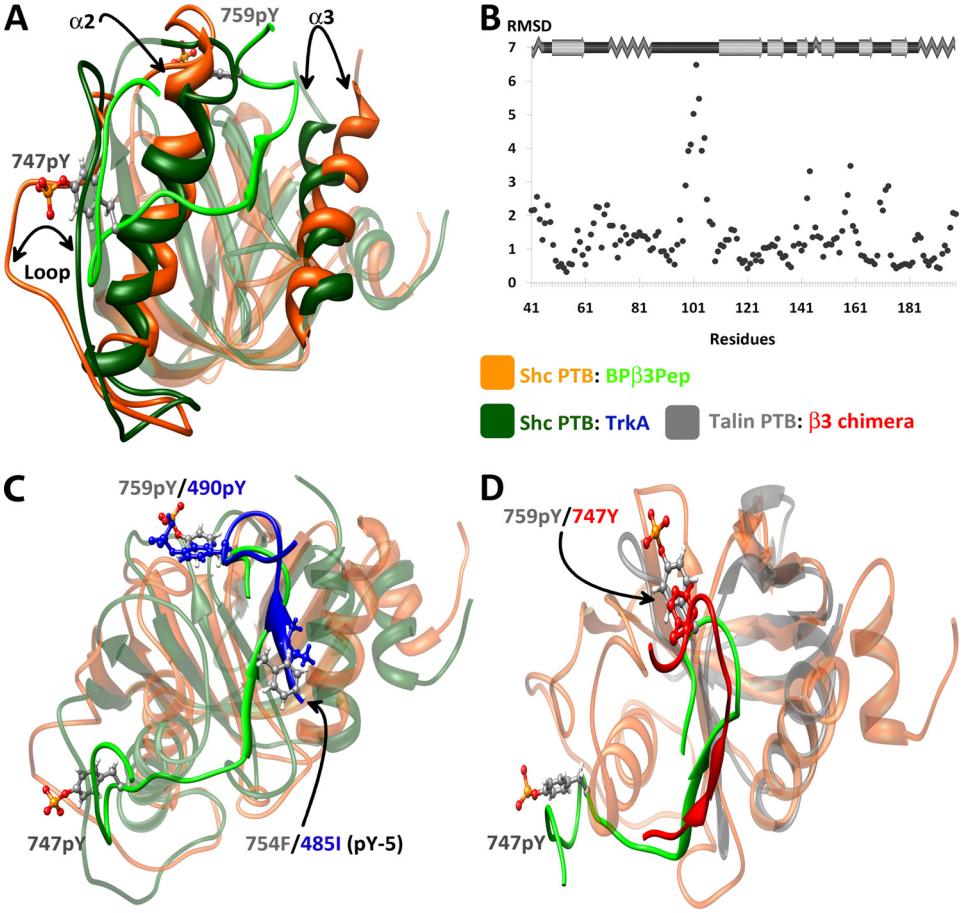

E

β1	732	KLLMIIHDRR EFAKFEKEKM	NAKWDTGENP	IYKSAVTTVV	---------NP	KYEGK----- ------	778
β2	702	KALIHLSDLR EYRRFEKEKL	KSQWNN-DNP	LFKSATTTVM	---------NP	KFAES----- ------	747
β3	716	KLLITIHDRK EFAKFEEERA	RAKWDTANNP	LYKEATSTFT	---------NI	TYRGT----- ------	762
β5	720	KLLVTIHDRR EFAKFQSERS	RARYEMASNP	LYRKPISTHT	VDFTFNKFNK	SYNGTVD--- ------	776
β6	710	KLLVSFHDRK EVAKFEAERS	KAKWQTGTNP	LYRGSTSTFK	---------NV	TYKHREKQKV DLSTDC	757
β7	728	RLSVEIYDRR EYSRFEKEQQ	QLNWKQDSNP	LYKSAITTTI	---------NP	RFQEADSPTL ------	779

FIGURE 6. **Comparison of Shc PTB-BPβ_3Peptide complex with Shc PTB-TrkA (PDB ID:1SHC) and TalinF3-β_3 chimera (PDB ID: 1MK7).** Molecular graphics images were produced using the UCSF Chimera package (42). Disordered regions (Shc PTB: 17–36, 203–207, and BPβ_3Peptide 736–739) are excluded for the sake of clarity. *A*, superimposition of the Shc PTB-BPβ_3Peptide complex (shown in *solid/transparent orange ribbons*) with Shc PTB-TrkA complex (shown in *solid/transparent dark green ribbons*, TrkA peptide is not shown). The phosphorylated tyrosine residues (pY^{747}, pY^{759}) are shown with *ball and stick representation*. BPβ_3Peptide is shown in *lime*; (*B*) R.M.S.D. of backbone (residues 41–198) Cα atoms (Shc PTB-BPβ_3Peptide *versus* Shc PTB-TrkA) plotted as a function of the residue numbers. The overall R.M.S.D. to mean (residues 41–198) is 2.26 Å ± 0.98Å; however, regions such as helix α2, helix α3, and long Shc loop connecting strand β2 and helix α2 show high fluctuations as these regions are directly involved in interaction with BPβ_3Peptide. Secondary structural elements are represented *above* the plot; (*C*) superimposition of the Shc PTB-BPβ_3Peptide complex (shown in *transparent orange ribbons*) with Shc PTB-TrkA complex (shown in *transparent dark green ribbons*). BPβ_3Peptide is shown in *lime*, TrkA peptide is shown in *dark blue*; (*D*) comparison of the Shc PTB-BPβ_3Peptide complex (shown in *transparent orange ribbons*) with Talin F3-β_3 chimera complex (shown in *transparent gray ribbons*). BPβ_3Peptide is shown in *lime*; β_3 chimera (GSHM-^{739}WDTANNPLYKE^{749}) is shown in *dark red*. *E*, sequence alignment (produced by CLC Sequence Viewer) of human β integrin CTs; highly conserved residues are depicted in *pink* and least conserved are in *blue*. β_4 and β_8 CTs are omitted, even though β_4CT (pY^{1526}) has been shown to interact with Shc PTB (43), because β_4CT is ~1090 residues long and the divergent β_8CT clearly lacks the conserved NP*X*Y and N*X*XY motifs required to mediate Shc PTB interaction.

Tyr^{747} of β_3 chimera occupies the acidic, hydrophobic grove of talin PTB domain as compared with pY^{759} utilizing the strongly basic pocket of Shc PTB. This observation led to the hypothesis regarding the reduction in binding affinity for talin upon Tyr^{747} phosphorylation due to the obvious charge repulsion and some steric hindrance. Surprisingly, the actual measured reduction in affinity was found to be modest, only ~2-fold (38). Moreover, in a previous study (39), β_3 integrin exhibited strong affinity for PTB domains of 17 different proteins. In addition to β_3CT, the cytoplasmic domains of integrin β_{1A}, β_5, and β_7 also demonstrated some affinities to several of these PTB domains, reflecting the intrinsic flexibility of both the PTB fold and β integrins. Among the possible reasons for such indiscrimination is the exceptional conservation of NP*X*Y and N*X*XY motifs within β integrin tails (Fig. 6*E*), which along with other critical residues, coordinate integrin-PTB domains interactions. However, considering the specific nature of Shc PTB: β_3CT interaction, we speculate that among all the integrin tails depicted in Fig. 6*E*, similar interaction with Shc PTB can be expected only in case of the tyrosine-phosphorylated β_6 (^{740}NVTpY^{743}) due to the presence of large hydrophobic residue, Phe^{738}, at pY-5 position. This bulky, hydrophobic residue (corresponding to Phe^{754} in β_3CT and Ile^{485} in TrkA, Fig. 6*C*) occupies the non-polar pocket formed between α3 helix and β5 strand of Shc PTB. Furthermore, according to our Shc PTB-BPβ_3Peptide complex, the placement of a large negative group (pT^{753}) next to this pY-5 residue should cause the charge repulsion with the nearby Thr^{75} (from α2 helix of Shc PTB) along with steric hindrance with the above mentioned non-polar pocket. This is probably the most likely cause for the decreased affinity (40) of β_3CT to Shc PTB observed upon Thr^{753} phosphorylation.

Overall, this presented comparison establishes two salient features: (i) proteins containing PTB fold can fine-tune their affinity toward their targets by an introduction of additional target-specific binding sites as the second phosphotyrosine-binding site defined in Shc; and (ii) integrin cytoplasmic tails are capable of accommodating different structural features depending upon the binding partner. This remarkable dexterity may be the underlying foundation for the crucial bidirectional flow of information through integrins. Although β_3CT interaction with Shc PTB is unique as compared with its interaction with talin or Dok1 PTB domains, a low sequence homology among PTB domains makes it is very difficult to predict whether the other PTB domains will interact

with β integrin tails in a manner similar to Shc, talin, or Dok1. Indeed, such low sequence homology within the PTB domains simultaneously presents a challenge for the computational modeling and an opportunity for the comprehensive structural investigation.

To conclude, we have (i) confirmed the direct Shc PTB interaction with β_3 integrin cytoplasmic tail; (ii) demonstrated that this interaction depends strongly on the tyrosine(s) phosphorylation state of the receptor; (iii) structurally characterized Shc PTB in complex with bi-phosphorylated β_3CT; and (iv) defined molecular details of the secondary non-canonical phosphotyrosine-binding site within the Shc PTB. Because Shc is involved in regulating the stimulation of VEGF production in tumor cells, our data help to understand how tyrosine phosphorylation of β_3 integrin is linked to MAPK pathway and how it may play multiple roles in the regulation of integrin signal transduction.

Acknowledgments—We thank Frank Delaglio for NMRPipe, NMRDraw, and Talos+ software and the CCPN-Analysis, Cyana, and UCSF-Chimera crews for patiently answering all our questions.

REFERENCES

1. Hynes, R. O. (2002) *Cell* **110,** 673–687
2. Vinogradova, O., Velyvis, A., Velyviene, A., Hu, B., Haas, T., Plow, E., and Qin, J. (2002) *Cell* **110,** 587–597
3. Vinogradova, O., Vaynberg, J., Kong, X., Haas, T. A., Plow, E. F., and Qin, J. (2004) *Proc. Natl. Acad. Sci. U.S.A.* **101,** 4094–4099
4. Schaffner-Reckinger, E., Gouon, V., Melchior, C., Plançon, S., and Kieffer, N. (1998) *J. Biol. Chem.* **273,** 12623–12632
5. Jenkins, A. L., Nannizzi-Alaimo, L., Silver, D., Sellers, J. R., Ginsberg, M. H., Law, D. A., and Phillips, D. R. (1998) *J. Biol. Chem.* **273,** 13878–13885
6. Phillips, D. R., Prasad, K. S., Manganello, J., Bao, M., and Nannizzi-Alaimo, L. (2001) *Curr. Opin. Cell Biol.* **13,** 546–554
7. Law, D. A., DeGuzman, F. R., Heiser, P., Ministri-Madrid, K., Killeen, N., and Phillips, D. R. (1999) *Nature* **401,** 808–811
8. Cowan, K. J., Law, D. A., and Phillips, D. R. (2000) *J. Biol. Chem.* **275,** 36423–36429
9. Pelicci, G., Lanfrancone, L., Grignani, F., McGlade, J., Cavallo, F., Forni, G., Nicoletti, I., Grignani, F., Pawson, T., and Pelicci, P. G. (1992) *Cell* **70,** 93–104
10. Ravichandran, K. S. (2001) *Oncogene* **20,** 6322–6330
11. Wary, K. K., Mainiero, F., Isakoff, S. J., Marcantonio, E. E., and Giancotti, F. G. (1996) *Cell* **87,** 733–743
12. Zhou, M. M., Ravichandran, K. S., Olejniczak, E. F., Petros, A. M., Meadows, R. P., Sattler, M., Harlan, J. E., Wade, W. S., Burakoff, S. J., and Fesik, S. W. (1995) *Nature* **378,** 584–592
13. Zhou, M. M., Meadows, R. P., Logan, T. M., Yoon, H. S., Wade, W. S., Ravichandran, K. S., Burakoff, S. J., and Fesik, S. W. (1995) *Proc. Natl. Acad. Sci. U.S.A.* **92,** 7784–7788
14. Higashi, T., Yoshioka, A., Shirakawa, R., Tabuchi, A., Nishioka, H., Kita, T., and Horiuchi, H. (2004) *Biochem. Biophys. Res. Commun.* **322,** 700–704
15. DiNitto, J. P., and Lambright, D. G. (2006) *Biochim. Biophys. Acta* **1761,** 850–867
16. De, S., Razorenova, O., McCabe, N. P., O'Toole, T., Qin, J., and Byzova, T. V. (2005) *Proc. Natl. Acad. Sci. U.S.A.* **102,** 7589–7594
17. Farooq, A., Zeng, L., Yan, K. S., Ravichandran, K. S., and Zhou, M. M. (2003) *Structure* **11,** 905–913
18. Ikura, M., Clore, G. M., Gronenborn, A. M., Zhu, G., Klee, C. B., and Bax, A. (1992) *Science* **256,** 632–638
19. Zwahlen, C., Legault, P., Vincent, S. J., Greenblatt, J., Konrat, R., and Kay, l. E. (1997) *J. Am. Chem. Soc.* **119,** 711–721
20. Delaglio, F., Grzesiek, S., Vuister, G. W., Zhu, G., Pfeifer, J., and Bax, A. (1995) *J. Biomol. NMR* **6,** 277–293
21. Hoch, J. C., and Stern, A. S. (1996) *NMR Data Processing*, Wiley-Interscience
22. Vranken, W. F., Boucher, W., Stevens, T. J., Fogh, R. H., Pajon, A., Llinas, M., Ulrich, E. L., Markley, J. L., Ionides, J., and Laue, E. D. (2005) *Proteins* **59,** 687–696
23. Farrow, N. A., Zhang, O., Szabo, A., Torchia, D. A., and Kay, L. E. (1995) *J. Biomol. NMR* **6,** 153–162
24. Shen, Y., Delaglio, F., Cornilescu, G., and Bax, A. (2009) *J. Biomol. NMR* **44,** 213–223
25. Güntert, P. (2004) *Methods Mol. Biol.* **278,** 353–378
26. Linge, J. P., Williams, M. A., Spronk, C. A., Bonvin, A. M., and Nilges, M. (2003) *Proteins* **50,** 496–506
27. Brünger, A. T., Adams, P. D., Clore, G. M., DeLano, W. L., Gros, P., Grosse-Kunstleve, R. W., Jiang, J. S., Kuszewski, J., Nilges, M., Pannu, N. S., Read, R. J., Rice, L. M., Simonson, T., and Warren, G. L. (1998) *Acta Crystallogr. D Biol. Crystallogr* **54,** 905–921
28. Matsuo, H., Walters, K. J., Teruya, K., Tanaka, T., Gassner, G. T., Lippard, S. J., Kyogoku, Y., and Wagner, G. (1999) *J. Am Chem. Soc.* 9903–9904
29. Kosen, P. A. (1989) in *Methods in Enzymology* (Oppenheimer, N. J., and James, T. L. eds), pp. 86–121, Academic Press, New York
30. Mahoney, N. M., Rastogi, V. K., Cahill, S. M., Girvin, M. E., and Almo, S. C. (2000) *J. Am. Chem. Soc.* **122,** 7851–7852
31. Legate, K. R., and Fässler, R. (2009) *J. Cell Sci.* **122,** 187–198
32. Calderwood, D. A., Zent, R., Grant, R., Rees, D. J., Hynes, R. O., and Ginsberg, M. H. (1999) *J. Biol. Chem.* **274,** 28071–28074
33. Garcia-Alvarez, B., de Pereda, J. M., Calderwood, D. A., Ulmer, T. S., Critchley, D., Campbell, I. D., Ginsberg, M. H., and Liddington, R. C. (2003) *Mol. Cell* **11,** 49–58
34. Anthis, N. J., Haling, J. R., Oxley, C. L., Memo, M., Wegener, K. L., Lim, C. J., Ginsberg, M. H., and Campbell, I. D. (2009) *J. Biol. Chem.* **284,** 36700–36710
35. Phillips, D. R., Nannizzi-Alaimo, L., and Prasad, K. S. (2001) *Thromb. Haemost.* **86,** 246–258
36. Ravichandran, K. S., Zhou, M. M., Pratt, J. C., Harlan, J. E., Walk, S. F., Fesik, S. W., and Burakoff, S. J. (1997) *Mol. Cell. Biol.* **17,** 5540–5549
37. Uhlik, M. T., Temple, B., Bencharit, S., Kimple, A. J., Siderovski, D. P., and Johnson, G. L. (2005) *J. Mol. Biol.* **345,** 1–20
38. Oxley, C. L., Anthis, N. J., Lowe, E. D., Vakonakis, I., Campbell, I. D., and Wegener, K. L. (2008) *J. Biol. Chem.* **283,** 5420–5426
39. Calderwood, D. A., Fujioka, Y., de Pereda, J. M., Garcia-Alvarez, B., Nakamoto, T., Margolis, B., McGlade, C. J., Liddington, R. C., and Ginsberg, M. H. (2003) *Proc. Natl. Acad. Sci. U.S.A.* **100,** 2272–2277
40. Kirk, R. I., Sanderson, M. R., and Lerea, K. M. (2000) *J. Biol. Chem.* **275,** 30901–30906
41. Porollo, A. A., Adamczak, R., and Meller, J. (2004) *Bioinformatics* **20,** 2460–2462
42. Pettersen, E. F., Goddard, T. D., Huang, C. C., Couch, G. S., Greenblatt, D. M., Meng, E. C., and Ferrin, T. E. (2004) *J. Comput. Chem.* **25,** 1605–1612
43. Dans, M., Gagnoux-Palacios, L., Blaikie, P., Klein, S., Mariotti, A., and Giancotti, F. G. (2001) *J. Biol. Chem.* **276,** 1494–1502